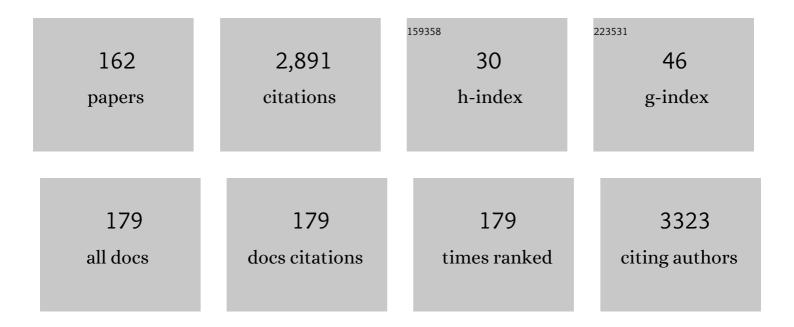
Christoph Koch

List of Publications by Year in descending order

Source: https://exaly.com/author-pdf/4303243/publications.pdf Version: 2024-02-01



#	Article	IF	CITATIONS
1	Band-gap measurements of direct and indirect semiconductors using monochromated electrons. Physical Review B, 2007, 75, .	1.1	103
2	A flux-preserving non-linear inline holography reconstruction algorithm for partially coherent electrons. Ultramicroscopy, 2008, 108, 141-150.	0.8	94
3	Confined and Chemically Flexible Grain Boundaries in Polycrystalline Compound Semiconductors. Advanced Energy Materials, 2012, 2, 992-998.	10.2	84
4	Resonant wedge-plasmon modes in single-crystalline gold nanoplatelets. Physical Review B, 2011, 83, .	1.1	81
5	FAIR data enabling new horizons for materials research. Nature, 2022, 604, 635-642.	13.7	81
6	Direct imaging of surface plasmon resonances on single triangular silver nanoprisms at optical wavelength using low-loss EFTEM imaging. Optics Letters, 2009, 34, 1003.	1.7	77
7	Intergranular glassy films: An overview. Materials Science & Engineering A: Structural Materials: Properties, Microstructure and Processing, 2006, 422, 3-18.	2.6	74
8	SESAM: Exploring the Frontiers of Electron Microscopy. Microscopy and Microanalysis, 2006, 12, 506-514.	0.2	72
9	An efficient, simple, and precise way to map strain with nanometer resolution in semiconductor devices. Applied Physics Letters, 2010, 96, .	1.5	69
10	Off-axis and inline electron holography: A quantitative comparison. Ultramicroscopy, 2010, 110, 460-471.	0.8	63
11	Off-axis and inline electron holography: Experimental comparison. Ultramicroscopy, 2010, 110, 472-482.	0.8	59
12	Quantitative analysis of layering and in-plane structural ordering at an alumina–aluminum solid–liquid interface. Acta Materialia, 2011, 59, 4378-4386.	3.8	58
13	Towards full-resolution inline electron holography. Micron, 2014, 63, 69-75.	1.1	55
14	Hybridized Metal Slit Eigenmodes as an Illustration of Babinet's Principle. ACS Nano, 2011, 5, 6701-6706.	7.3	54
15	Method for Retrieval of the Three-Dimensional Object Potential by Inversion of Dynamical Electron Scattering. Physical Review Letters, 2012, 109, 245502.	2.9	53
16	Grain-boundary types in chalcopyrite-type thin films and their correlations with film texture and electrical properties. Thin Solid Films, 2009, 517, 2545-2549.	0.8	49
17	Aberration-compensated large-angle rocking-beam electron diffraction. Ultramicroscopy, 2011, 111, 828-840.	0.8	49
18	The Structure of Grain Boundaries in Strontium Titanate: Theory, Simulation, and Electron Microscopy. Annual Review of Materials Research, 2010, 40, 557-599.	4.3	47

#	Article	IF	CITATIONS
19	Atomic scale confirmation of ferroelectric polarization inversion in wurtzite-type AlScN. Journal of Applied Physics, 2021, 129, .	1.1	46
20	Electron energy losses in Ag nanoholes—from localized surface plasmon resonances to rings of fire. Optics Letters, 2009, 34, 2150.	1.7	44
21	Wedge Dyakonov Waves and Dyakonov Plasmons in Topological Insulator Bi ₂ Se ₃ Probed by Electron Beams. ACS Nano, 2016, 10, 6988-6994.	7.3	43
22	Strain mapping along Al–Pb interfaces. Acta Materialia, 2010, 58, 162-172.	3.8	41
23	Direct imaging of the electron liquid at oxide interfaces. Nature Nanotechnology, 2018, 13, 198-203.	15.6	40
24	Evolution of order in amorphous-to-crystalline phase transformation of MgF ₂ . Journal of Applied Crystallography, 2013, 46, 1105-1116.	1.9	39
25	General framework for quantitative three-dimensional reconstruction from arbitrary detection geometries in TEM. Physical Review B, 2013, 87, .	1.1	39
26	Direct Quantification of Ordering at a Solid-Liquid Interface Using Aberration Corrected Transmission Electron Microscopy. Physical Review Letters, 2013, 110, 086106.	2.9	38
27	Iterative phase retrieval without support. Optics Letters, 2004, 29, 2737.	1.7	37
28	Hybridization approach to in-line and off-axis (electron) holography for superior resolution and phase sensitivity. Scientific Reports, 2014, 4, 7020.	1.6	37
29	Analysis of Cu(In,Ca)(S,Se)2 thin-film solar cells by means of electron microscopy. Solar Energy Materials and Solar Cells, 2011, 95, 1452-1462.	3.0	35
30	Projected potential profiles across interfaces obtained by reconstructing the exit face wave function from through focal series. Ultramicroscopy, 2006, 106, 525-538.	0.8	34
31	The role of plasmons and interband transitions in the color of AuAl2, AuIn2, and AuGa2. Applied Physics Letters, 2011, 99, 111908.	1.5	31
32	Influence of Silicon Layers on the Growth of ITO and AZO in Silicon Heterojunction Solar Cells. IEEE Journal of Photovoltaics, 2020, 10, 703-709.	1.5	31
33	Crystal Growth and Real Structure Effects of the First Weak 3D Stacked Topological Insulator Bi ₁₄ Rh ₃ I ₉ . Chemistry of Materials, 2013, 25, 2359-2364.	3.2	30
34	Silver nanowires with optimized silica coating as versatile plasmonic resonators. Scientific Reports, 2019, 9, 3859.	1.6	29
35	In Situ TEM Monitoring of Phase-Segregation in Inorganic Mixed Halide Perovskite. Journal of Physical Chemistry Letters, 2020, 11, 4945-4950.	2.1	29
36	Mapping of valence energy losses via energy-filtered annular dark-field scanning transmission electron microscopy. Ultramicroscopy, 2009, 109, 1164-1170.	0.8	28

#	Article	IF	CITATIONS
37	Breaking the Mode Degeneracy of Surface Plasmon Resonances in a Triangular System. Langmuir, 2012, 28, 8867-8873.	1.6	28
38	Atomic signatures of local environment from core-level spectroscopy in <mml:math xmlns:mml="http://www.w3.org/1998/Math/MathML"><mml:mrow><mml:mi>î²</mml:mi><mml:mtext>â^'mathvariant="normal">O<mml:mn>3</mml:mn></mml:mtext></mml:mrow>. Physical Review B, 2016, 94, .</mml:math 	nl:mtext> 1.1	<mml:msub>< 28</mml:msub>
39	Imaging dislocation cores – the way forward. Philosophical Magazine, 2006, 86, 4781-4796.	0.7	27
40	A nondamaging electron microscopy approach to map In distribution in InGaN light-emitting diodes. Journal of Applied Physics, 2010, 108, .	1.1	27
41	Linking Microstructure and Nanochemistry in Human Dental Tissues. Microscopy and Microanalysis, 2012, 18, 509-523.	0.2	27
42	FDES, a GPU-based multislice algorithm with increased efficiency of the computation of the projected potential. Ultramicroscopy, 2015, 158, 89-97.	0.8	26
43	Overcoming information reduced data and experimentally uncertain parameters in ptychography with regularized optimization. Optics Express, 2020, 28, 28306.	1.7	24
44	High- <i>k</i> 2D Sb ₂ O ₃ Made Using a Substrate-Independent and Low-Temperature Liquid-Metal-Based Process. ACS Nano, 2021, 15, 16067-16075.	7.3	24
45	From Fully Strained to Relaxed: Epitaxial Ferroelectric Al _{1â€} <i>_x</i> Sc <i>_x</i> N for Illâ€N Technology. Advanced Functional Materials, 2022, 32, .	7.8	24
46	Microstructure, chemistry, and electronic structure of natural hybrid composites in abalone shell. Micron, 2013, 48, 54-64.	1.1	22
47	Origins of electrostatic potential wells at dislocations in polycrystalline Cu(In,Ga)Se2 thin films. Journal of Applied Physics, 2014, 115, .	1.1	22
48	Gold―and Silverâ€Coated Barium Titanate Nanocomposites as Probes for Twoâ€Photon Multimodal Microspectroscopy. Advanced Functional Materials, 2019, 29, 1904289.	7.8	22
49	Stacked-Bloch-wave electron diffraction simulations using GPU acceleration. Ultramicroscopy, 2014, 141, 32-37.	0.8	21
50	Metal-Assisted and Solvent-Mediated Synthesis of Two-Dimensional Triazine Structures on Gram Scale. Journal of the American Chemical Society, 2020, 142, 12976-12986.	6.6	21
51	Toward quantitative core-loss EFTEM tomography. Ultramicroscopy, 2011, 111, 1255-1261.	0.8	20
52	Self-Assembly of Plasmonic Nanoantenna–Waveguide Structures for Subdiffractional Chiral Sensing. ACS Nano, 2021, 15, 351-361.	7.3	20
53	Third-dimension information retrieval from a single convergent-beam transmission electron diffraction pattern using an artificial neural network. Physical Review B, 2014, 89, .	1.1	18
54	Correlative Highâ€Resolution Mapping of Strain and Charge Density in a Strained Piezoelectric Multilayer. Advanced Materials Interfaces, 2015, 2, 1400281.	1.9	18

#	Article	IF	CITATIONS
55	Poly(ionic liquid) Nanovesicle-Templated Carbon Nanocapsules Functionalized with Uniform Iron Nitride Nanoparticles as Catalytic Sulfur Host for Li–S Batteries. ACS Nano, 2022, 16, 10554-10565.	7.3	18
56	A useful expansion of the exponential of the sum of two non-commuting matrices, one of which is diagonal. Journal of Physics A, 2003, 36, 803-816.	1.6	17
57	Multi-resolution convolutional neural networks for inverse problems. Scientific Reports, 2020, 10, 5730.	1.6	17
58	EFTEM study of surface plasmon resonances in silver nanoholes. Ultramicroscopy, 2010, 110, 1094-1100.	0.8	16
59	Microstructure and Elastic Constants of Transition Metal Dichalcogenide Monolayers from Friction and Shear Force Microscopy. Advanced Materials, 2018, 30, e1803748.	11.1	16
60	Spatial Phase Distributions in Solution-Based and Evaporated Cs–Pb–Br Thin Films. Journal of Physical Chemistry C, 2019, 123, 17666-17677.	1.5	16
61	Inversion of dynamical electron scattering to obtain the crystal potential using data from two thicknesses. Acta Crystallographica Section A: Foundations and Advances, 2001, 57, 473-474.	0.3	14
62	Pulsed thermal deposition of binary and ternary transition metal dichalcogenide monolayers and heterostructures. Applied Physics Letters, 2019, 114, .	1.5	14
63	Strain mapping of LED devices by dark-field inline electron holography: Comparison between deterministic and iterative phase retrieval approaches. Ultramicroscopy, 2013, 127, 119-125.	0.8	13
64	Quantitative Analysis of HAADF–STEM Images of MoVTeTaO M1 Phase Catalyst for Propane Ammoxidation to Acrylonitrile. ChemCatChem, 2015, 7, 3731-3737.	1.8	13
65	Stepâ€byâ€step synthesis of copper(I) complex supported on platinum nanoparticleâ€decorated mesoporous silica hollow spheres and its remarkable catalytic performance in Sonogashira coupling reaction. Applied Organometallic Chemistry, 2020, 34, e5645.	1.7	13
66	Modelling of HREM and nanodiffraction for dislocation kinks and core reconstruction. Journal of Physics Condensed Matter, 2000, 12, 10175-10183.	0.7	12
67	Highâ€Resolution Mapping of Strain Partitioning and Relaxation in InGaN/GaN Nanowire Heterostructures. Advanced Science, 2022, 9, .	5.6	12
68	Study of coherence strain of GP II zones in an aged aluminum composite. Journal of Alloys and Compounds, 2012, 536, S159-S164.	2.8	11
69	A three-dimensional polarization domain retrieval method from electron diffraction data. Ultramicroscopy, 2015, 155, 42-48.	0.8	11
70	Inverse dynamical photon scattering (IDPS): an artificial neural network based algorithm for three-dimensional quantitative imaging in optical microscopy. Optics Express, 2016, 24, 7006.	1.7	11
71	Neural-network-based depth-resolved multiscale structural optimization using density functional theory and electron diffraction data. Physical Review B, 2018, 97, .	1.1	11
72	Surface-Functionalized Au–Pd Nanorods with Enhanced Photothermal Conversion and Catalytic Performance. ACS Applied Materials & Interfaces, 2022, 14, 17259-17272.	4.0	11

#	Article	IF	CITATIONS
73	Investigation of the electrostatic potential of a grain boundary in Y-substituted BaZrO3 using inline electron holography. Physical Chemistry Chemical Physics, 2019, 21, 17662-17672.	1.3	10
74	Removal of supporting amorphous carbon film induced artefact from measured strain variation within a nanoparticle. Ultramicroscopy, 2019, 199, 70-80.	0.8	10
75	Stationary beam full-field transmission helium ion microscopy using sub-50 keV He ⁺ : Projected images and intensity patterns. Beilstein Journal of Nanotechnology, 2019, 10, 1648-1657.	1.5	10
76	Composition analysis and transition energies of ultrathin Sn-rich GeSn quantum wells. Physical Review Materials, 2020, 4, .	0.9	10
77	A consistent picture of excitations in cubic BaSnO3 revealed by combining theory and experiment. Communications Materials, 2022, 3, .	2.9	10
78	Charge-Trapping-Induced Compensation of the Ferroelectric Polarization in FTJs: Optimal Conditions for a Synaptic Device Operation. IEEE Transactions on Electron Devices, 2022, 69, 3694-3699.	1.6	10
79	The evolution of amorphous grain boundaries during in-situ heating experiments in Lu–Mg doped Si3N4. Materials Science & Engineering A: Structural Materials: Properties, Microstructure and Processing, 2006, 422, 92-101.	2.6	9
80	Determination of grain boundary potentials in ceramics: Combining impedance spectroscopy and inline electron holography. International Journal of Materials Research, 2010, 101, 43-49.	0.1	9
81	Correlating the structural, chemical, and optical properties at nanometer resolution. Journal of Applied Physics, 2010, 107, 013501.	1.1	9
82	A practical way to resolve ambiguities in wavefront reconstructions by the transport of intensity equation. Ultramicroscopy, 2015, 154, 1-6.	0.8	9
83	Inversion of Dynamical Scattering from Large-Angle Rocking-Beam Electron Diffraction Patterns. Physical Review Letters, 2016, 117, 015501.	2.9	9
84	Mapping the electrostatic potential of Au nanoparticles using hybrid electron holography. Ultramicroscopy, 2016, 165, 8-14.	0.8	9
85	On the measurement of dislocation core periods by nanodiffraction. The Philosophical Magazine: Physics of Condensed Matter B, Statistical Mechanics, Electronic, Optical and Magnetic Properties, 2001, 81, 1701-1711.	0.6	8
86	Atomic String Holography. Physical Review Letters, 2001, 86, 5510-5513.	2.9	8
87	Retrieving depth-direction information from TEM diffraction data under reciprocal-space sampling variation. Ultramicroscopy, 2015, 148, 105-114.	0.8	8
88	Extra half-plane shortening of dislocations as an origin of tensile strain in Si-doped (Al)GaN. Journal of Applied Physics, 2019, 126, .	1.1	8
89	Various Compressed Sensing Setups Evaluated Against Shannon Sampling Under Constraint of Constant Illumination. IEEE Transactions on Computational Imaging, 2019, 5, 502-514.	2.6	8
90	Large Area Ultrathin InN and Tin Doped InN Nanosheets Featuring 2D Electron Gases. ACS Nano, 2022, 16, 5476-5486.	7.3	8

#	Article	IF	CITATIONS
91	Extrinsic Localized Excitons in Patterned 2D Semiconductors. Advanced Functional Materials, 0, , 2203060.	7.8	8
92	Observation of electronic Raman scattering from Mg-doped wurtzite GaN. Applied Physics Letters, 2000, 76, 2889-2891.	1.5	7
93	Solving non-centrosymmetric two-dimensional crystal structures by dynamic electron diffraction. Acta Crystallographica Section A: Foundations and Advances, 2005, 61, 231-236.	0.3	7
94	Recovering low spatial frequencies in wavefront sensing based on intensity measurements. Advanced Structural and Chemical Imaging, 2016, 2, .	4.0	7
95	Strain-induced indium clustering in non-polar a-plane InGaN quantum wells. Acta Materialia, 2018, 145, 109-122.	3.8	7
96	Angle-Resolved Electron Energy Loss Spectroscopy. Microscopy and Microanalysis, 2020, 26, 964-965.	0.2	7
97	High-Fidelity 4D-STEM Enabled by Live Processing at 15'000 Detector Frames Per Second. Microscopy and Microanalysis, 2021, 27, 994-997.	0.2	7
98	Solving the Phase Problem for Electron Diffraction of Non-Centrosymmetric Two-Dimensional Organic Crystals Using the Example of Membrane Proteins. Microscopy and Microanalysis, 2004, 10, 414-415.	0.2	6
99	Aspects regarding measurement of thickness of intergranular glassy films. Journal of Microscopy, 2006, 221, 46-62.	0.8	6
100	Determining the radial pair-distribution function within intergranular amorphous films by numerical nanodiffraction. Ultramicroscopy, 2006, 106, 383-388.	0.8	6
101	Energy-filtered phase retrieval using the transport of intensity equation. Applied Physics Letters, 2011, 99, 221905.	1.5	6
102	Measuring three-dimensional positions of atoms to the highest accuracy with electrons. Comptes Rendus Physique, 2014, 15, 119-125.	0.3	6
103	Multi-focus TIE algorithm including partial spatial coherence and overlapping filters. Optics Express, 2018, 26, 11819.	1.7	6
104	A Three-Dimensional Reconstruction Algorithm for Scanning Transmission Electron Microscopy Data from a Single Sample Orientation. Microscopy and Microanalysis, 2022, 28, 1632-1640.	0.2	6
105	Experimental evidence for dislocation core structures in silicon. Scripta Materialia, 2001, 45, 1273-1278.	2.6	5
106	Projected Potential Profiles across Intergranular Glassy Films. Journal of the Ceramic Society of Japan, 2006, 114, 1005-1012.	1.3	5
107	Gradient flipping algorithm: introducing non-convex constraints in wavefront reconstructions with the transport of intensity equation. Optics Express, 2016, 24, 8344.	1.7	5
108	Measuring Electrostatic Potential Profiles across Amorphous Intergranular Films by Electron Diffraction. Microscopy and Microanalysis, 2006, 12, 160-169.	0.2	4

#	Article	IF	CITATIONS
109	VEELS band gap measurements using monochromated electrons. Journal of Physics: Conference Series, 2008, 126, 012005.	0.3	4
110	Using dynamically scattered electrons for three-dimensional potential reconstruction. Acta Crystallographica Section A: Foundations and Advances, 2009, 65, 364-370.	0.3	4
111	Strain mapping for advanced CMOS technologies. Crystal Research and Technology, 2014, 49, 38-42.	0.6	4
112	Simultaneous orientation and thickness mapping in transmission electron microscopy. Ultramicroscopy, 2015, 150, 37-43.	0.8	4
113	Comparison of Ptychography vs. Center-of-mass Analysis of Registered 4D-STEM Series. Microscopy and Microanalysis, 2020, 26, 1898-1900.	0.2	4
114	Individual tubular J-aggregates stabilized and stiffened by silica encapsulation. Colloid and Polymer Science, 2020, 298, 937-950.	1.0	4
115	Analysis of Local Charges at Hetero-interfaces by Electron Holography – A Comparative Study of Different Techniques. Ultramicroscopy, 2021, 231, 113236.	0.8	4
116	5D-STEM: Live processing and display at 15,000 diffraction patterns per second. Microscopy and Microanalysis, 2021, 27, 1064-1065.	0.2	4
117	AssessingThermodynamic Properties of Amorphous Nanostructures by Energy-Filtered Electron Diffraction. Microscopy and Microanalysis, 2004, 10, 254-255.	0.2	3
118	Examination of structural properties of interfaces by electron diffraction. Materials Science & Engineering A: Structural Materials: Properties, Microstructure and Processing, 2006, 422, 41-50.	2.6	3
119	Dynamic behavior of nanometer-scale amorphous intergranular film in silicon nitride by in situ high-resolution transmission electron microscopy. Journal of the European Ceramic Society, 2011, 31, 1835-1840.	2.8	3
120	Electron Holography: Correlative Highâ€Resolution Mapping of Strain and Charge Density in a Strained Piezoelectric Multilayer (Adv. Mater. Interfaces 1/2015). Advanced Materials Interfaces, 2015, 2, .	1.9	3
121	Inline electron holography and VEELS for the measurement of strain in ternary and quaternary (In,Al,Ga)N alloyed thin films and its effect on bandgap energy. Journal of Microscopy, 2016, 261, 27-35.	0.8	3
122	Design and application of a relativistic Kramers–Kronig analysis algorithm. Ultramicroscopy, 2019, 206, 112825.	0.8	3
123	Imaging grain boundary segregation by electron diffractive imaging. International Journal of Materials Research, 2005, 96, 443-447.	0.8	3
124	Mapping Grain Boundary Potentials by Inline Electron Holography. Microscopy and Microanalysis, 2007, 13, 334-335.	0.2	2
125	Application of Monochromated Electrons in EELS. Microscopy and Microanalysis, 2008, 14, 134-135.	0.2	2
126	Effect of surface orientation on intrinsic island formation on SrTiO ₃ surfaces. Journal of Physics: Conference Series, 2008, 94, 012013.	0.3	2

#	Article	IF	CITATIONS
127	Two-dimensional misorientation mapping by rocking dark-field transmission electron microscopy. Ultramicroscopy, 2015, 159, 26-33.	0.8	2
128	Raman shifts in MBEâ€grown Si x Ge 1 ⴒ  x  ⴒ  y Sn y alloys with large Si content. Journal of R Spectroscopy, 2021, 52, 1167-1175.	aman 1.2	2
129	Adaptive Scanning in Ptychography through Deep Reinforcement Learning. Microscopy and Microanalysis, 2021, 27, 818-821.	0.2	2
130	Software Precession Electron Diffraction. , 2008, , 201-202.		2
131	Kinetic Study on the Adsorption of 2,3,5,6-Tetrafluoro-7,7,8,8-tetracyanoquinodimethane on Ag Nanoparticles in Chloroform: Implications for the Charge Transfer Complex of Ag–F ₄ TCNQ. ACS Applied Nano Materials, 2021, 4, 11625-11635.	2.4	2
132	A Quantitative Nanodiffraction System for Ultrahigh Vacuum Scanning Transmission Electron Microscopy. Microscopy and Microanalysis, 2003, 9, 468-474.	0.2	1
133	Chemical bonds in damaged and pristine low- \hat{I}^{e} materials: A comparative EELS study. Microelectronic Engineering, 2008, 85, 2169-2171.	1.1	1
134	Damage-free Analysis of Biological Materials by Vibrational Spectroscopy in the EM. Microscopy and Microanalysis, 2020, 26, 108-110.	0.2	1
135	Quantifying the data quality of focal series for inline electron holography. Ultramicroscopy, 2021, 231, 113264.	0.8	1
136	Improving 4DSTEM measurements of atomic charge and electrostatic potential via energy filtration. Microscopy and Microanalysis, 2021, 27, 1450-1452.	0.2	1
137	Low-loss-energy EFTEM imaging of triangular silver nanoparticles. , 2008, , 243-244.		1
138	Features of Our SEM Transmission Diffraction Sub-stage with 6-axis Sample Control and a Camera with Variable Camera Length. Microscopy and Microanalysis, 2020, 26, 1906-1907.	0.2	1
139	Electronic Raman Scattering from Mg-Doped Wurtzite GaN. Materials Research Society Symposia Proceedings, 1999, 595, 1.	0.1	0
140	Numerical Nanodiffraction of Amorphous Grain Boundary Films. Microscopy and Microanalysis, 2003, 9, 44-45.	0.2	0
141	Determination of Projected Potential Profiles Across Interfaces Using Through Focal Series Reconstruction. Microscopy and Microanalysis, 2006, 12, 1016-1017.	0.2	0
142	Requisites for Ultimate Energy Resolution EELS and Band Gap Measurements. Microscopy and Microanalysis, 2006, 12, 1148-1149.	0.2	0
143	Analytical and high-resolution TEM investigation of Boron-doped CeO2. , 2008, , 565-566.		0

144 J. Spence's 65th birthday. Ultramicroscopy, 2011, 111, iii.

0.8 0

#	Article	IF	CITATIONS
145	Introduction to the special issue in honor of Regents' Prof. John C.H. Spence in occasion of his 65th birthday. Ultramicroscopy, 2011, 111, 745-746.	0.8	0
146	The Stuttgart Center for Electron Microscopy at the Max Planck Institute for Metals Research. International Journal of Materials Research, 2011, 102, 815-827.	0.1	0
147	Hybridization of Off-Axis and In-line High-Resolution Electron Holography. Microscopy and Microanalysis, 2014, 20, 272-273.	0.2	0
148	Interfaces and Extended Structural Defects in Chalcopyrite Thin-Film Solar Cells Studied by Transmission Electron Microscopy. Microscopy and Microanalysis, 2014, 20, 530-531.	0.2	0
149	Real-Space Simulation of Electron Scattering in Imperfect Crystals and Reconstruction of the Electrostatic Potential. Microscopy and Microanalysis, 2015, 21, 1883-1884.	0.2	0
150	Unconventional Surface Plasmon Excitations in Bi2Se3. Microscopy and Microanalysis, 2015, 21, 2057-2058.	0.2	0
151	Hybrid Electron Holography. Microscopy and Microanalysis, 2015, 21, 2311-2312.	0.2	0
152	Direct mapping of strain state in nonpolar InGaN/GaN multilayers using dark-field inline electron holography. , 2015, , .		0
153	Retrieving Atomic Structure from Dynamical Rocking Curve Measurements in both Real and Reciprocal Space. Microscopy and Microanalysis, 2016, 22, 920-921.	0.2	0
154	Correlative Microscopy Characterization of Cesium-Lead-Bromide Thin-films. , 2018, , .		0
155	Energy Transfer between Cyanoâ€Ether PPV and InGaN/GaN Quantum Wells with Large Piezoelectric Fields. Physica Status Solidi (A) Applications and Materials Science, 2018, 215, 1800322.	0.8	0
156	Direct Observation of Field-induced Modulation of Two-dimensional Electron Gas at Oxide Interfaces. Microscopy and Microanalysis, 2019, 25, 1848-1849.	0.2	0
157	Streamlining Processing and Utilization of EM Data - An Efficient Open-source Solution. Microscopy and Microanalysis, 2020, 26, 2946-2948.	0.2	0
158	Band gap mapping using monochromated electrons. , 2008, , 381-382.		0
159	Nonlinear Electron Inline Holography. , 2008, , 263-264.		0
160	Measuring electron scattering factors by large-angle rocking-beam electron diffraction (LARBED). Acta Crystallographica Section A: Foundations and Advances, 2010, 66, s66-s66.	0.3	0
161	Large-angle rocking-beam electron diffraction (LARBED). Acta Crystallographica Section A: Foundations and Advances, 2011, 67, C696-C697.	0.3	0
162	TEM-based analysis of the crystal structure of a Ge-rich layer sandwiched between spintronic Fe3Si. Acta Crystallographica Section A: Foundations and Advances, 2018, 74, e311-e311.	0.0	0